Turbulent Pulsating Nanofluids Flow and Heat Transfer inside Constant Heat Flux Boundary Condition Helical-Coil Tube

A. A. Abbasian Arani*, A. Jahani

Mechanical Engineering Department, University of Kashan, Kashan, Iran

ABSTRACT: Heat transfer enhancement has been the goal of many researches carried out over the past three decades. Employing the modified fluids, changing the flow geometry, and active methods are among the commonly used techniques. The effects of three referred techniques, employing pulsation flow as active method, nanofluids instead of conventional fluid as modified fluids and helical-coil tube as changing the flow geometry on the fluid flow and heat transfer have been investigated numerically. The results of interests with pulsation flow and non-pulsation flow have been presented. In this research, the results indicated that, the coil pitch tube and coil diameter have a minor effect on the Nusselt number (5 and 7%, respectively). But the Reynolds number has a major effect on the Nusselt number, so that by increasing the Reynolds number from 5000 to 100000, the Nusselt number will be enhanced by more than 200%. The nanofluid pressure drop and heat transfer coefficient increased with nanoparticles volume fraction. In addition, by introducing a concept as the performance evaluation criteria, the mutual effects of the pressure drop and Nusselt number were investigated with referred concept. Performance evaluation criteria revealed that employing the nanofluid in lower Reynolds numbers yields higher effects on the fluid flow and heat transfer.

1. INTRODUCTION

On the one hand, the size reduction of heat transfer systems, and the significant increase of heat production in the thermal equipment, on the other hand, encourage the researchers to focus on the devices with higher heat transfer in short time and high intensity. Nanofluid technology offers high potential for the development of high-performance cooling systems with the small and economical manners [1-8]. The application of nanoparticles offers an opportunities to achieve to the modify thermophysical properties (thermal conductivity) as well as better (higher) transfer properties (friction factor, convection heat transfer and Nusselt number). A large number of investigators [9-12] have carried out an extensive researches in this field and have shown that the nanofluids can realize the above objectives. Another method used to increase the heat transfer is using the helical-coil/spiral-coil tubes instead of direct tubes. Helical-coil/spiral-coil tubes are one of the most commonly used technique in the industrial heat transfer. The use of these tubes in heat exchangers not only improves their performance, but also reduces the size of the heat exchanger significantly. The efficiency of heat exchangers can also be increased by employing the active techniques. One of the active technique, is to create a shock in the fluid flow that increases the heat transfer. Pulse generators can be used to enhance the heat transfer rates. The pulsation flow increases

the heat transfer rate due to increasing the turbulent surfaces in the boundary layer. In the following, the previous studies on the heat transfer and pressure drop in a helical-coil/spiral-coil tube for a pulsation flow in the presence of nanofluids are reviewed and discussed.

Ramezani Kharvani et al. [13] analyzed empirically the heat transfer in a spiral-coil tube along with the flow of water as the working fluid in the turbulent flow regime. Their results showed that the highest increase in the overall heat transfer coefficients, for upstream and downstream of fluid flows is about 26% and 19%, respectively. They showed that use of pulse in the spiral-coil or straight tubes increases the heat transfer rate too. They attributed this enhancement to the production of turbulent flow, while generating a pulsation flow increases the required pumping power. Jun et al. [14] studied empirically the increase of heat transfer by pulsation flow to examine the effect of pulsation on the heat transfer rate. They concluded that, in general, the pulsation flow increases the heat transfer, because, it can break the thermal boundary layer on the wall, so the thermal resistance decreases. Doshmanziari et al. [15] studied the characteristics of heat transfer of water-alumina nanoparticles in a spiral-coil tube for turbulent flow regime. Their results indicated that, the heat transfer of the base fluid increases by replacing with the nanofluid or applying the pulsation to the flow. In addition, the pulsation can increase or decrease the heat transfer rates

*Corresponding author's email: email

of the fluid flow based on the impact frequency, flow rate and nanofluids concentration. Zohir et al. [16] studied the heat transfer and pressure drop inside an annuli equipped with coiled wires in turbulent flow regime. Their results showed that the highest rate of increase in the Nusselt number compared to that of the smooth ring without pulsation was about 12.7, while the friction coefficient was about 8.7 times in the same conditions. In this research, an experimental relationship was proposed, that provides the Nusselt number in terms of different parameters with a maximum deviation of 13% too. Hassanzadeh Afrouzi et al. [17] studied the fluid flow and heat transfer in a helical-coil tube considering constant heat flux boundary condition. Their results showed that the frequency has an important effect on the heat transfer rate. The Nusselt number also increased dramatically by increasing the pulse range. However, the twisting step has no significant effect on the fluid flow and heat transfer characteristics. Based on their report, the curvature ratio is a key parameter in the flow field and heat transfer in such tubes. They also reported that, the average Nusselt number decreased with increasing the curvature ratio and increased by increasing the curvature ratio. Patro et al. [18] conducted a numerical study to predict the heat transfer in pulsating turbulent flow regime. The results showed that for a special frequency and Reynolds number, the local Nusselt number decreases along the tube with partial oscillation. Naphon and Wiriyasart [19] examined the heat transfer of water-titanium dioxide nanofluid in a pulsed stream inside the spiral-coil tubes with different magnetic fields. Pulse frequency and magnetic field have an important effect on the heat transfer enhancement. They also showed that the pulsation flow Nusselt number is higher than that the continuous one, while the pulsation flow and the applied magnetic field slightly increase the friction coefficient. Sivasankaran and Narin [20] investigated numerically the two-phase pulsating nanofluid flow in the spiral microchannel in the presence of porous media. They reported that, the pulse input flow will be able to increase the convection heat transfer substantially with an average of 6%. In addition, the Nusselt number increases with decreasing the power due to increasing the mixing, and also the thermal performance coefficient increases with increasing the frequency. Rahgoshay et al. [21] investigated the nanofluid pulsation flow in laminar flow regime inside a curved tube with constant heat flux boundary condition. They showed that increasing the amplitude and frequency resulted in a slight increase in the Nusselt number, but a higher rate of heat transfer was observed with increasing the Reynolds number and nanoparticles volume fraction. Ishino et al. [22] studied the effect of pulsating on the fluid flow and heat transfer by varying the three parameters, the amplitude, the frequency and the mean velocity under constant wall temperature boundary condition. Their results showed that the Nusselt number decreases initially with increasing the amplitude and then recover gradually and finally increase much greater than original values. They concluded that in the pulsation flow with non-zero mean velocity pulsation cannot always promote the heat transfer, but sometimes suppresses it, depending mainly

on the pulsation mean velocity and amplitude. Elshafei et al. [23] published a numerical research on the fluid flow and heat transfer of pulsation air flow in turbulent flow regime with uniform tube wall heat flux as boundary condition. The results of this study indicated that the values of Nusselt number are increased and decreased depending to the applied frequency in pulsation flow compared with steady-state flow. Jarrahi and Castelain [24] examined the patterns of secondary flow and composition in a laminar pulsating flow in a coil-tube. The effects of independent parameters such as velocity, Womersley number and Reynolds number on the secondary flow structure were studied and the secondary flow was analyzed at zero, 90, and 180 degrees of fuzzy positions. Selimefendigil and Öztop [25] analyzed the effects of the fuzzy shift on the heat transfer properties during the pulsating mixed convection in a multiple vented cavity. Their research showed that the heat transfer is affected by changing the independent parameters as phase shift and Richardson number. Wang and Zhang [26] conducted a numerical analysis on the heat transfer in the turbulent flow regime inside the coil-tube. Their investigation shown that, the Womersley number is a key parameter in this type of flow and heat transfer. Their results indicated that, in the pulsating turbulent flow, there is a special Womersley number, in which the heat transfer achieved maximum value.

By reviewing and summarizing the recent investigations, it has been found that a little studies have been carried out on the fluid flow and heat transfer inside the coiled tubes considering the effect of pulsating flows in the presence of nanofluids. In this work, the flow field and heat transfer of pulsating turbulent flow regime of water-Al_2O_3 nanofluid inside the helical-coil tube was studied numerically.

2. NUMERICAL MODELING

In this section, the problem geometry, considerations of the flow regime, the system of governing equations, the working fluid properties, the turbulence criteria, the fluid and thermal boundary conditions, and the numerical simulation of straight and coiled-tube with pulsating and non-pulsating flows have been presented. In the following, the calculation of heat transfer coefficient, pressure drop, Performance Evaluation Criteria (PEC), and developed region length are presented to simulate the fluid flow and heat transfer inside the tube.

2-1-Physical model

The schematic diagram and geometric profile of the helical-coil tube are shown in Fig. 1. Geometric characteristics of helical-coil include: coil diameter (D), coil step (pitch) (P), and coil inner diameter (d). In Table 1, the geometric characteristics of the studied helical-coil tube in this research are presented. In this research, the Al_2O_3-water nanofluids flow inside the coiled-tube is simulated numerically in different flow regime and geometric configuration.

2-2-System of governing equations in turbulent flow regime

The system of governing equations for the incompressible viscous fluid flow and heat transfer inside the helical-coil tube
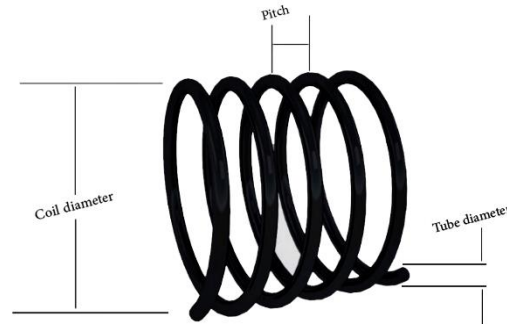
Fig. 1. Geometry of helical-coil tube

Table 1. Characteristics geometry of helical-coil tube

Characteristic	Symbol	Value
Inner diameter	d_i	9 mm
Pitch	P	18 mm
Coil diameter	D	116 mm
Number of coil	N	10

are presented as follows:

$$\frac{\partial}{\partial x_i}\left(\rho u_i\right) = 0 \tag{1}$$

$$\frac{\partial}{\partial x_j}\left(\rho u_i u_j\right) = -\frac{\partial P}{\partial x_i} + \frac{\partial}{\partial x_j}\left(\mu\left(\frac{\partial u_i}{\partial x_j} + \frac{\partial u_j}{\partial x_i}\right)\right) + \frac{\partial}{\partial x_j}\left(-\rho\overline{u_i'u_j'}\right), \tag{2}$$

$$\frac{\partial}{\partial x_i}\left(\rho u_i T\right) = \frac{\partial}{\partial x_j}\left(\left(\Gamma + \Gamma_t\right)\frac{\partial T}{\partial x_j}\right), \tag{3}$$

where, ρ is the fluid density, u_i is the velocity component of the fluid, μ, u'_i and u_j, are the fluid viscosity, the oscillating part of fluid velocity and the fluid velocity, respectively. In addition, $-\rho\overline{u_i'u_j'}$, is the average turbulent shear stress. Using the Reynolds's similarity analysis, the term "average turbulent shear stress" can also be obtained. In other words, in order to simulate the fluid flow and heat transfer in the turbulent flow, an expression for the turbulent shear stress needs to be presented. In addition, Γ and Γ_t are the molecular thermal diffusivity and turbulent thermal diffusivity, respectively and are given by

$$\Gamma = \frac{\mu}{Pr}, \qquad \Gamma_t = \frac{\mu_t}{Pr_t}, \tag{4}$$

Here, k-ε turbulence model is used to continue the solving the problem. Based on this model, using the Boussinesq hypothesis, the relationship between the average turbulent shear stress known as Reynolds stresses is proposed as follows:

$$\left(-\rho\overline{u_i'u_j'}\right) = \mu_t\left(\frac{\partial u_i}{\partial x_j} + \frac{\partial u_j}{\partial x_i}\right), \tag{5}$$

In the recent term μ_t, the so-called turbulent viscosity coefficient or eddy viscosity, is calculated using a suitable turbulence model, which can be modeled as follows:

$$\mu_t = \rho C_\mu \frac{k^2}{\varepsilon}, \tag{6}$$

where k and ε are obtained from the kinetic energy of turbulence and the kinetic energy losses respectively using the following equations:

$$u_i\frac{\partial k}{\partial x_i} = \frac{\partial}{\partial x_i}\left(\left(\mu + \frac{\mu_t}{\sigma_k}\right)\frac{\partial k}{\partial x_i}\right) + G_k - \rho\varepsilon, \tag{7}$$

$$u_i\frac{\partial\varepsilon}{\partial x_i} = \frac{\partial}{\partial x_i}\left(\left(\mu + \frac{\mu_t}{\sigma_\varepsilon}\right)\frac{\partial\varepsilon}{\partial x_i}\right) + C_{1\varepsilon}\frac{\varepsilon}{k}G_k - C_{2\varepsilon}\frac{\varepsilon^2}{k}\rho, \tag{8}$$

where, G_k is the generated turbulent kinetic energy due to the velocity gradient:

$$G_k = -\rho\overline{u_i'u_j'}\frac{\partial u_j}{\partial u_i}. \tag{9}$$

$C_{1\varepsilon}$ and $C_{2\varepsilon}$ are constant and σ_k and σ_ε are turbulent prandtl numbers of k and ε respectively, which are presented in the Table 2. With averaging from the variables, the Reynolds stress and then the eddy viscosity are obtained. Effective viscosity for the turbulent flow is obtained from the fluid viscosity and eddy viscosity.

2-3-Boundary condition

The boundary conditions on the inlet of helical-coil tube, are considered to be pulsating flow. The boundary conditions on the outlet of helical-coil tube, are considered as pressure equal to zero (atmosphere pressure). The

Table 2. Constants used in the *k-ε* turbulence model [27, 28]

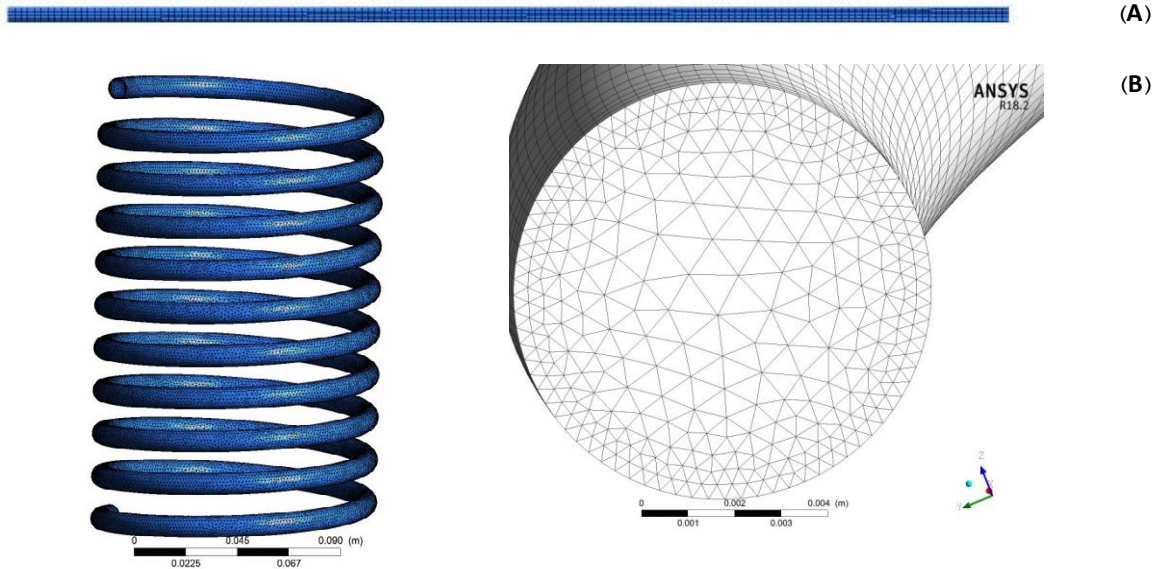| C_μ	$C_{1\varepsilon}$	$C_{2\varepsilon}$	σ_K	σ_ε	σ_t
0.09	1.44	1.92	1	1.3	1

Fig. 2. The grid used in the grid independence test. A) Straight tube B) Helical-coil tube

boundary conditions on the tube wall, are also fixed as constant heat flux equal to 922 W/m² for heat transfer, and non-slip boundary condition for fluid flow and heat transfer. Therefore, the inlet flow velocity is a periodic function of time and is defined as:

$$U(t) = U_m + U_A \sin 2\pi f t, \tag{10}$$

where, U_m is the average flow velocity, the U_A is the amplitude and *f* is flow frequency of the fluid flow. In addition, the inlet temperature was fixed at 300 K.

3. SIMULATION METHOD AND GRID GENERATION

Preparing the appropriate grid and solving the system of governing equations of fluid flow and heat transfer of the nanofluid in the straight tube and helical-coil tube were performed using the ANSYS FLUENT software version 15. In the energy and momentum equations, a second-order upwind scheme is used to discretize the convection term, and to discretize the turbulence equations, the first-order upwind scheme is employed. To obtain the convergent response, the used under relaxation coefficient is 0.7 for momentum equations and 0.8 for energy and turbulence equations.

The grid created by the software for simulating the 2 Dimensional (2D) straight tube and the 3D simulation of the coiled tube is shown in Fig. 2. For this propose, the size of the grid along the wall should be small enough. To do this purpose, in the straight tube the Bias factor is considered to

be 3 in the direction of radius. The length of the straight tube is 1200 mm and the tube diameter is 15.5 mm. To find the proper grid, air flow into the straight tube for *Re* = 22300, *L* = 1200 mm and *d* = 15.5 mm with constant heat flux boundary conditions was applied.

In addition, the velocity distribution with radios in a cross section inside the straight tube for various element number is provided in Fig. 3. As can be seen with increasing the element number from the 2250 to 3750 the variation in velocity is negligible.

In the Tables 3 and 4, the heat transfer coefficient and the pressure drop for the turbulent flow regime are shown for the straight and coiled tubes respectively. As can be seen from the Table 3, the change in heat transfer coefficient and pressure drop from the element number of 2250 to 3750 is small, so the grid number of 2250 elements is considered for straight tube.

To determine the proper grid, fluid flow of water flow inside the coiled tube for *Re* = 12600, *d* = 9 mm and *D* = 116 mm, with constant heat flux as boundary conditions is applied. For coiled tube similar manner were used. A grid with the number of elements equal to 993856 was considered for the coiled tube. In addition, the value of grid's *y⁺* was between 32 and 94 (Table 4).

3-1-Validation

In order to validation, the fluid flow of air in the straight tube and the fluid flow of water inside of coiled tube is simulated and compared with selected references.
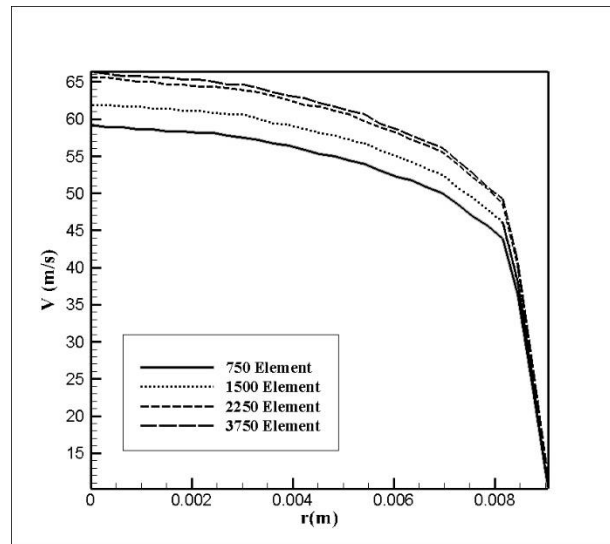
Fig. 3. Velocity distribution in cross section of straight tube with radios for various element numbers Fig. 4. Comparison between the results of present simulation for the coefficient of performance in the straight tube with the data of Elshafei et al. [29] at *f*=13.3 Hz.

Table 3. Heat transfer coefficient and pressure drop for different grids for straight tube

Number of grids	Δp (Pa)	$h\left(\mathrm{W/m^2.K}\right)$
750	155.0	207.5
1500	159.0	208.0
2250	160.0	208.0
3750	160.0	208.4

Table 4. Heat transfer coefficient and pressure drop for different grids for coiled tube

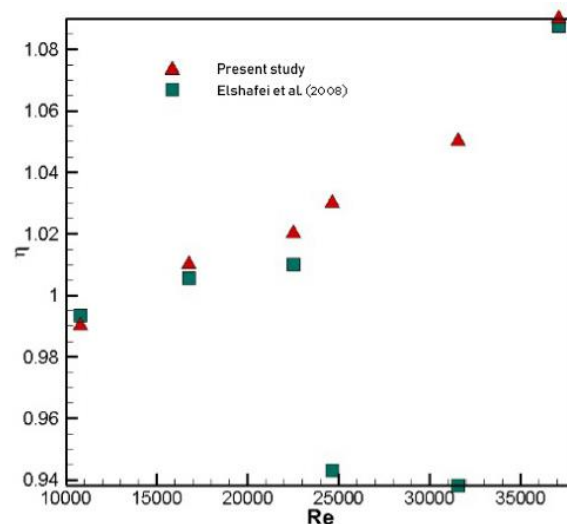| Number of grids	Δp (Pa)	$h\left(\mathrm{W/m^2.K}\right)$
495124	1541087	67.0
758479	1591258	71.0
993856	1671944	78.0
1507921	1672012	78.0

Fig. 4. Comparison between the results of present simulation for the coefficient of performance in the straight tube with the data of Elshafei et al. [29] at f=13.3 Hz.

3-1-1-Pulsating flow inside straight tube

In order to validate the numerical results, the results of simulation of the present study are compared with the results of Elshafei et al. [29]. They conducted a numerical and experimental study to measure the pulsating airflow efficiency coefficient. They performed their test under the constant heat flux boundary conditions. In Fig. 4, the simulation results of present investigation for the straight tube with pulsating flow are compared with the data of Elshafei et al. [29]. As can be seen, the simulation results of present study are relatively
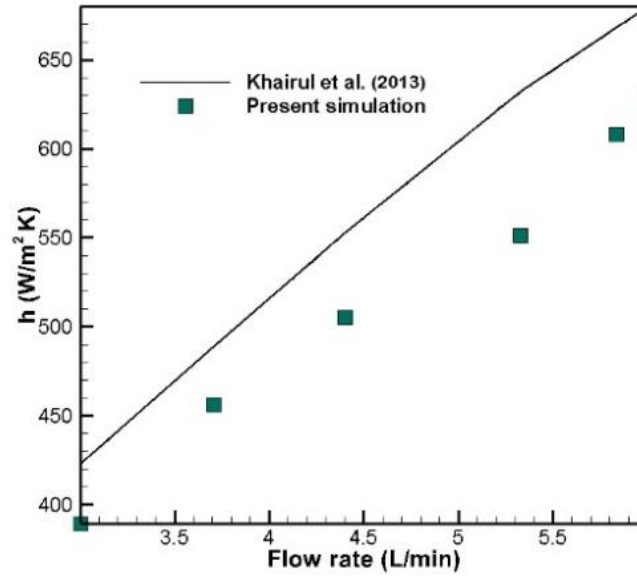
Fig. 5. Comparison between the present numerical simulation results for the heat transfer coefficient of coiled tube with the numerical results of Khairul et al. [30] for un-pulsation flow.

close to the experimental data with acceptable accuracy. The minimum and maximum deviations are 0.2% and 11.9% respectively. Based on the exist comparison between the numerical study and experimental data reported in the literature, the obtained deviation is in the accepted range.

3-1-2- Un-pulsating flow inside coiled tube

In order to validate the results, the results of the present numerical simulation are compared with the numerical results of Khairul et al. [30]. Their numerical investigation has been conducted for a coiled tube with the constant heat flux boundary condition. In Fig. 5, the simulation results of present study for the average Nusselt number are compared with the numerical results of Khairul et al. [30] in term of Reynolds number. The numerical simulation conditions are considered to be the same with the numerical investigation of Khairul et al. [30]. As can be seen, the numerical results of present simulation have a fairly good accuracy when it compared with the numerical results of Khairul et al. [30]. Maximum and minimum deviation is 6% and 12%, respectively.

4. DATA PROCESSING
4-1-Total heat transfer coefficient

The average temperature at each tube section for the constant heat flux boundary condition is linear as follows:

$$T_{bx} = \frac{\dot{q}\pi d_i Lx}{\dot{m}c_p} + T_{bi} ,$$ (11)

The local heat transfer coefficient for the tube with the constant heat flux boundary conditions is as follows:

$$h_x(t) = \frac{\dot{q}}{T_{sx} - T_{bi}} ,$$ (12)

where T_{bi} and T_{sx} are the fluid input average temperature (bulk temperature) and the tube wall temperature, respectively.

The average heat transfer coefficient in terms of time is obtained from the following equation:

$$h(t) = \frac{1}{L}\int h_x(t)dx .$$ (13)

The total heat transfer coefficient is obtained by time integrating in a pulsating flow period [31]:

$$h = f\int_0^{1/f} h_x(t)dt ,$$ (14)

where f is the pulsating flow frequency.

The total Nusselt number is as follows:

$$Nu = \frac{hd_i}{k} .$$ (15)

The nondimensional frequency of turbulent flow is defined as [29]:

$$\omega^* = \frac{\omega d_i}{U^*} .$$ (16)

where ω is the angular pulsation frequency, given by [29]:

$$\omega = 2\pi f .$$ (17)

and U^* is the friction velocity defined as [32]:

$$U^* = 0.199 U_m / Re^{0.125} .$$ (18)

For helical-coil tubes, instead of the Reynolds number, the Dean number is used similar to Reynolds number, and is defined as:

$$De = Re(\frac{d}{D})^{1/2}. \tag{19}$$

The critical Reynolds number and the Dean number of the helical-coil tube are as follows [33]:

$$Re_{cr} = 2000 (d / D_C)^{0.32}, \tag{20}$$

$$De_{cr} = 2000(d / D_C)^{0.82}. \tag{21}$$

The Reynolds number in term of mass flow rate is defined as:

$$Re = \frac{4\dot{m}}{\pi d_o \mu}. \tag{22}$$

4-2-Pressure drop

The pressure drop inside the duct having the hydraulic diameter D_h, and the tube length of L is obtained from the Darcy equation as follow:

$$\Delta p = f_d \frac{L}{D_h} \frac{\rho V^2}{2}, \tag{23}$$

where f_d is the average friction factor. As it can be seen from this equation, the determination of the pressure drop inside the duct is depends on the average friction factor, which the average friction factor depends on the flow regime, the geometrical shape of the duct and the hydrodynamic length from the inlet.

4-3-Performance coefficient criteria

Two types of efficiency indexes (named as performance evaluation criteria, PEC) which are based on the comparison between the applying of pulsation flow instead the steady flow, and the other related to the using the nanofluid instead of the base fluid are presented, respectively as [34]:

$$\eta = \frac{\left(h_{pulsation} / h_{steady-state}\right)}{\left(\Delta p_{pulsation} / \Delta p_{steady-state}\right)}, \tag{24}$$

$$\eta = \frac{\left(h_{nanofluid} / h_{base\ fluid}\right)}{\left(\Delta p_{nanofluid} / \Delta p_{base\ fluid}\right)}. \tag{25}$$

5. NANOFLUID PROPERTIES
5-1-Thermal conductivity coefficient

By using a regression analysis on the several valid experimental data, Corcione [35] presented the following experimental correlation with the maximum error of 1.86% for nanofluid thermal conductivity:

$$\frac{k_{nf}}{k_f} = 1 + 4.4 Re^{0.4} Pr^{0.66} (\frac{T}{T_{fr}})^{10} (\frac{k_p}{k_f})^{0.03} \phi^{0.66}, \tag{26}$$

where, Re is the nanoparticles Reynolds number, Pr is the base fluid prandtl number, T is the nanoparticle temperature in K, T_{fr} is the base fluid freezing temperature in K, k_p is the nanoparticles thermal conductivity, k_f is the base fluid thermal conductivity, and φ is the nanoparticles volume fraction. The thermal conductivity of the base fluid (water) and the aluminum oxide nanoparticles are 0.59 W/m.K and 40 W/m.K, respectively.

The nanoparticles Reynolds number is defined as:

$$Re = \frac{\rho_f u_B d_p}{\mu_f}, \tag{27}$$

where ρ_f and μ_f are the density and viscosity of the base fluid, respectively. d_p and u_B represent the nanoparticles diameter and average Brownian velocity, respectively. Brownian velocity of nanoparticles u_B is the ratio of d_p and the required time to traverse this distance (Brownian motion penetration time). Brownian's penetration time is obtained as follows:

$$t_B = \frac{\pi \mu d_p^3}{2 k_B T}, \tag{28}$$

where k_B is the Boltzmann constant. So:

$$u_B = \frac{2 k_B T}{\pi \mu_f d_p^2}. \tag{29}$$

By replacing the Eq. (29) in Eq. (27), the nanoparticles Reynolds number is obtained as follows:

$$Re = \frac{2 \rho_f k_B T}{\pi \mu_f d_p}. \tag{30}$$

The Corcione [35] correlation covers a wide range of nanoparticles including aluminum oxide, copper oxide, titanium oxide and copper, and the base fluids including water and ethylene glycol, the nanoparticle diameter is in the range of 10 nm to 150 nm, the nanoparticles volume fractions ranging from 0.002 to 0.9 and the temperature range from 294 to 324 K.

5-2-Dynamic viscosity

Corcione [35] used a regression analysis on the valid exist experimental data and presented the following experimental correlation for the viscosity prediction with the maximum deviation of 1.86%.

$$\frac{\mu_{nf}}{\mu_f} = \frac{1}{1 - 34.87(d_p / d_f)^{-0.3} \phi^{1.03}}, \tag{31}$$

where d_f is the molecules diameter of the base fluid which is defined as follows:

$$d_f = 0.1 \left(6M / N \pi \rho_{f_0}\right)^{1/3}, \tag{32}$$

where M is the base molecular mass, N is the Avogadro number, and ρ_{f_0} is the density of the base fluid at the temperature of $T_0 = 293$ K. It should be noted that the viscosity of the base fluid (water) is obtained from the following equation:
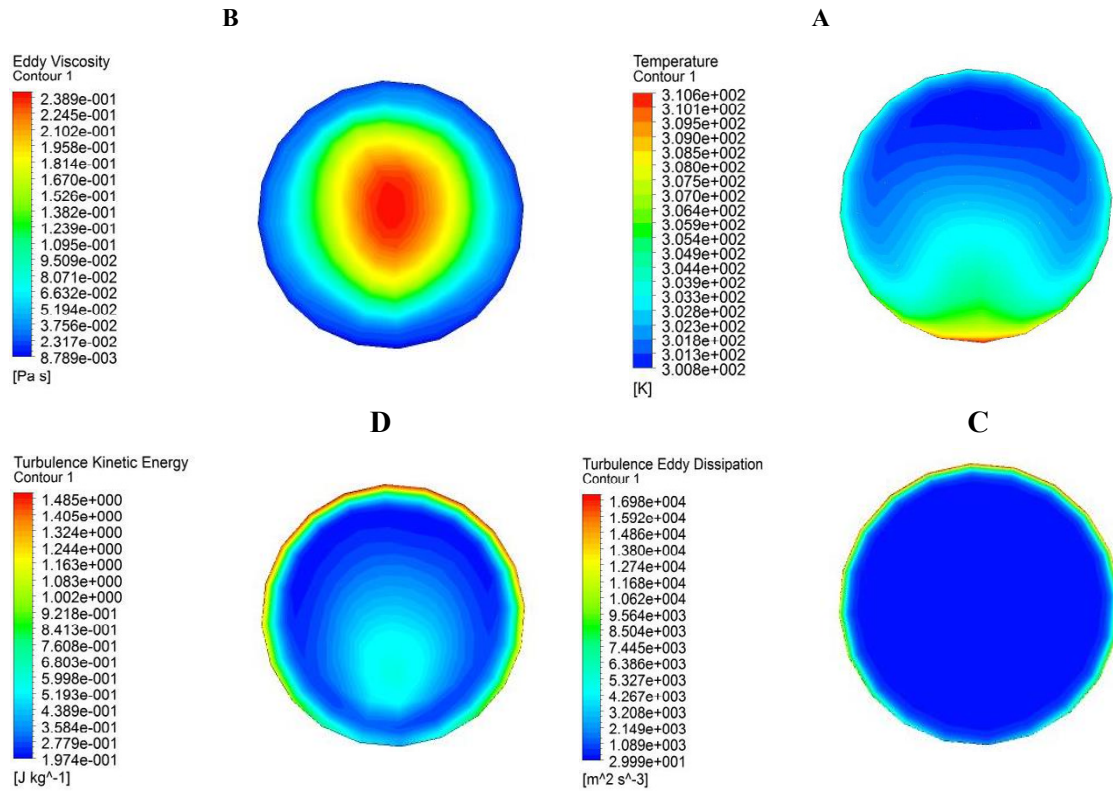
B

Eddy Viscosity
Contour 1

2.389e-001
2.245e-001
2.102e-001
1.958e-001
1.814e-001
1.670e-001
1.526e-001
1.382e-001
1.239e-001
1.095e-001
9.509e-002
8.071e-002
6.632e-002
5.194e-002
3.756e-002
2.317e-002
8.789e-003

[Pa s]

A

Temperature
Contour 1

3.106e+002
3.101e+002
3.095e+002
3.090e+002
3.085e+002
3.080e+002
3.075e+002
3.070e+002
3.064e+002
3.059e+002
3.054e+002
3.049e+002
3.044e+002
3.039e+002
3.033e+002
3.028e+002
3.023e+002
3.018e+002
3.013e+002
3.008e+002

[K]

D

Turbulence Kinetic Energy
Contour 1

1.485e+000
1.405e+000
1.324e+000
1.244e+000
1.163e+000
1.083e+000
1.002e+000
9.218e-001
8.413e-001
7.608e-001
6.803e-001
5.998e-001
5.193e-001
4.389e-001
3.584e-001
2.779e-001
1.974e-001

[J kg^-1]

C

Turbulence Eddy Dissipation
Contour 1

1.698e+004
1.592e+004
1.486e+004
1.380e+004
1.274e+004
1.168e+004
1.062e+004
9.564e+003
8.504e+003
7.445e+003
6.386e+003
5.327e+003
4.267e+003
3.208e+003
2.149e+003
1.089e+003
2.999e+001

[m^2 s^-3]

Fig. 6. Contour on the helical-coil tube exit. A) The temperature contour. B) The eddy viscosity; C) The eddy dissipation; and D) The turbulence kinetic energy

$$\mu_f = 562.77\left(Ln\left(T + 62.756\right)\right)^{-8.9137} \tag{33}$$

5-3-Density and specific heat capacity

To calculate the density and specific constant pressure heat capacity of the nanofluid, Ho et al. [36] proposed the following equation derived from the mixture theory:

$$\rho_{nf} = \left(1 - \phi\right)\rho_f + \phi\rho_p, \tag{34}$$

$$c_{pnf} = \frac{\left(1 - \phi\right)\left(\rho c_p\right)_f + \phi\left(\rho c_p\right)_p}{\left(1 - \phi\right)\left(\rho\right)_f + \phi\left(\rho\right)_p}. \tag{35}$$

5-4-Length of the developed region

During a laminar flow, the length of the hydrodynamic and thermal developing regions are approximated through the following equations [37]:

$$\frac{X/D}{Re} \cong 0.04, \tag{36}$$

$$X_T = Pr.X. \tag{37}$$

These lengths in turbulent flow regimes can be obtained from the following equation:

$$\frac{X}{D} \cong 10 \cong \frac{X_T}{D}, \tag{38}$$

According to Eq. (38), the maximum length of the hydrodynamic and thermal developing region of the turbulent flow is about 155 mm in straight tube, and 90 mm in coil tube. As can be seen the length of straight tube is 1500 mm and the coil tube is about 3650 mm. Due to presented information, fully developed flow and heat transfer condition is exist in the straight tube and in the coil tube.

6. RESULTS AND DISCUSSION

In this work, the fluid flow and heat transfer of water/ aluminum oxide nanofluid inside the helical-coil tube in turbulent flow regime was simulated numerically. A parametric study, including the effects of Reynolds number, frequency, pulse amplitude and helical coil geometry characteristic on the fluid flow and heat transfer has been examined. The pulsating flow enters the tube at 300 K. The heat flux on the wall is fixed at 100000 W/m². The output boundary condition is fixed at zero pressure. The results are obtained with the Reynolds number ranging between 5000 and 100000, the frequency between 5 and 50, and the amplitude ranging from 0.1 to 0.5 times the average speed.

6-1-Steady state flow simulation
6-1-1- Temperature contours

The temperature contour, the eddy viscosity, the eddy dissipation, and the turbulence kinetic energy at the exit point of the helical-coil tube are shown in Fig. 6. As can be seen from the Fig. 6, the temperature near the wall and the
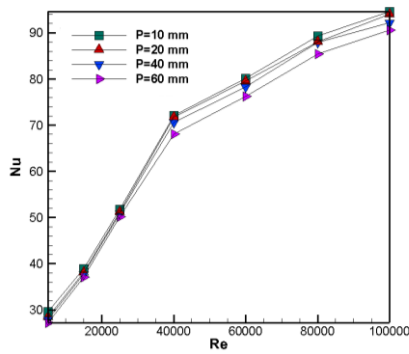
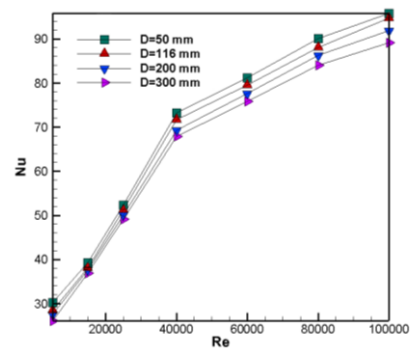**Fig. 7. Variation of Nusselt number with Reynolds number for various coil pitch**

Fig. 8. Variation of Nusselt number with Reynolds number for various coil diameter

secondary vortices, which has the highest displacement due to secondary vortices, is the highest. The eddy dissipation and the turbulence kinetic energy are also the smallest in the vicinity of the secondary vortices.

6-1-2- Helical-coil tube pitch effect on the fluid flow and heat transfer

The variation of Nusselt number with Reynolds number at various pitch value are presented in Fig. 7. As can be seen from the Fig. 7, as the pitch increases, the Nusselt number decreases. As the pitch is increased, the curvature effect of the coil decreases and the effect of secondary vortices decreases too.

By reducing the effect of vortices, the heat transfer will be also reduced, and as a consequence, the Nusselt number decrease. The obtained result of present investigation shows that with a pitch increment from 10 to 60 mm in the Reynolds number of 5000, the reduction of Nusselt number is small, and by increasing the Reynolds number to 100000, this decrease reaches to the maximum value of 5%. As the Reynolds number increases, the Nusselt number increases too, as well as changes in the Nusselt number with the coil pitch (5% maximum in 10 mm coil pitch) (Fig. 7).

When the Reynolds number increased from 5000 to 100000, the Nusselt number enhance from 28 to 95, which represents an increase of about 240% for a coil pitch of 10 mm. The increase of the Nusselt number for coils with other pitches have similar trend, because the change in the Nusselt number with the coil pitch, as presented at the beginning of this section, is negligible. In addition, as can be seen the effect of Reynolds number is greater than pitch value. In fact, with increasing the pitch, the effect of curvature is reduced, but the variation of Nusselt number with Reynolds number cover the effect of pitch values. Referred phenomenon is due the negligible effect of pitch value in comparison with the effect of Reynolds number on Nusselt number.

In fact, in investigated flow and heat transfer conditions, the fluid flow and heat transfer is affected mainly from the Reynolds number, and changing the geometry has not important effect on the fluid flow and heat transfer. On the other hand, increasing the Reynolds number increased the

fluid activity that provided higher Nusselt number.

6-1-3- Coil diameter effect on the fluid flow and heat transfer

The variation of Nusselt number with Reynolds number at various coil diameter are presented in Fig. 8. As can be seen from the Fig. 8, as the diameter increases, the Nusselt number decreases. As the diameter is increased, the curvature effect of the coil decreases and the effect of secondary vortices decreases too. By reducing the effect of vortices, the heat transfer will be reduced also, and thus the Nusselt number will decrease. Variation of Nusselt number with diameter for each Reynolds number in studied diameter range is small. As the Reynolds number increases, the variation of Nusselt number with diameter increases. The difference in the Nusselt number for the Reynolds number of 100000 with the diameters of 50 mm and 300 mm is about 6.5%. As the Reynolds number increases, the Nusselt number increases also, as well as the changes in the Nusselt number with the coil diameter. When the Reynolds number increases from 5000 to 100000, the Nusselt number increase from 30 to 95; an increase of about 210% for a diameter of 50 mm. Similar trend for Nusselt number for other diameters is observed.

Fig. 9 show the effect of Reynolds number variation on the ratio of the Nusselt number of nanofluid to that of the base fluid flows in the helical-coil tube, the pressure drop ratio and the performance coefficient criteria for the water/aluminum oxide nanofluid.

The pressure drop and the Nusselt number of the nanofluid decrease in comparison to their respective values for the base fluid by increasing the Reynolds number. Increasing the Reynolds number increases the secondary circulation stream power and the power of the turbulent flow, and intensifies the gradient of the near-wall velocity. Therefore, the effect of nanoparticles on the increasing the pressure drop and the Nusselt number, relative to the Reynolds number for the helical-coil tube, decreases, especially in comparison with the effect of increasing the mixing effect or convection, due to increasing the turbulent flow or secondary vortices. As the nanoparticles volume fraction increases, the ratio of pressure drop and Nusselt number increases, and decreases with increasing the Reynolds number. In the lower Reynolds

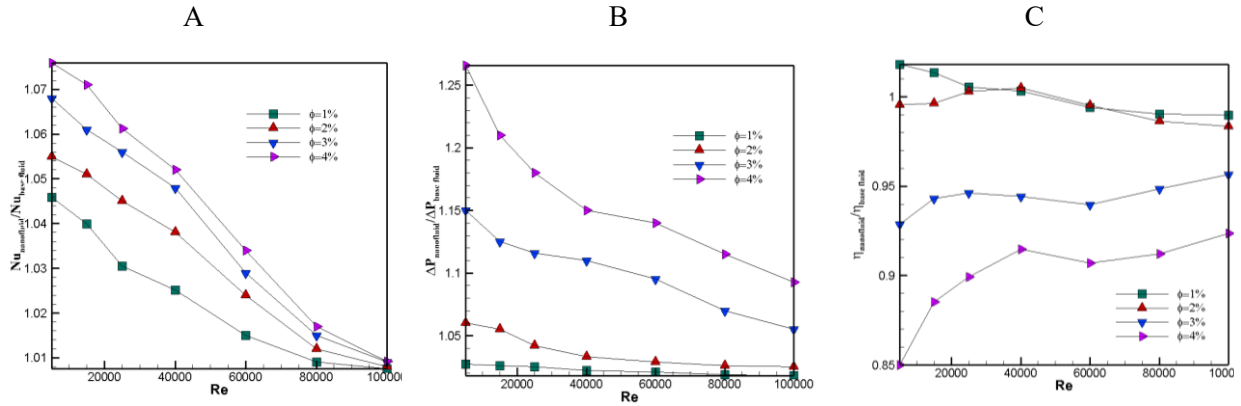A   B   C

Fig. 9. A) Nanofluid Nusselt number to that of the base fluid ratio variation, B) Nanofluid pressure drop to that of base fluid ratio variation, C) Nanofluid performance evaluation criteria to that of the base fluid variation with Reynolds number for various water/ aluminum oxide nanofluid nanoparticle volume fraction flowing inside the helical-coil tube for *d* = 9 mm and *D* = 112 mm.

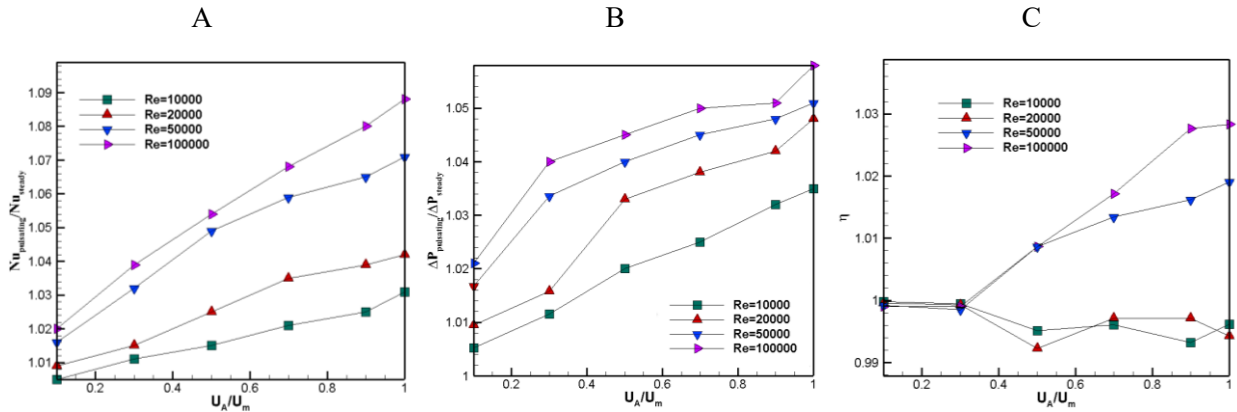A   B   C

Fig. 10. A) The Nusselt number of pulsation flow to that of steady-state ratio variation, B) the pressure drop of pulsation flow to that of steady-flow variation, and C) thermal performance criteria with the ratio of the flow amplitude to that of the mean flow for various Reynolds number of water flow inside the helical-coil tube for *d* = 9 mm and *D* = 112 mm.

numbers, the performance coefficient increases with increasing the Reynolds number, then decreases and then increases. Therefore, in a particular Reynolds number, there is an optimal performance coefficient that determines the best point. By increasing the nanoparticles volume fraction, the performance coefficient decreases. Reduction of the performance coefficient by increasing the nanoparticles volume fraction is due to the increasing in the pressure drop.

6-2. Pulsating flow simulation
6-2-1. The effect of flow amplitude

In Fig. 10, the ratio of Nusselt number of pulsating flow to that of the steady flow, the ratio of the pressure gradient of pulsating flow to that of the steady flow, and the efficiency with the ratio of the flow amplitude to that of the mean flow for various Reynolds number are shown. By increasing the amplitude ratio, the Nusselt number ratio and the pressure drop ratio increase.

The performance coefficient for the lower Reynolds numbers is decreasing and lower than 1, and for the higher

Reynolds numbers is increasing and higher than 1.

6-2-2. Effect of frequency

In Fig. 11, the variation of the Nusselt number with time is shown for two frequencies of 10 and 50 Hz.

As the frequency of the input flow increases, the frequency of the Nusselt number increases and the range of Nusselt numbers decreases. The reason for the Nusselt number decrease, is the increase in the integral area which is due to the increase in frequency. The effect of flow frequency on the ratio of the Nusselt number in the pulsating flow to the Nusselt number in the steady-state flow (Fig. 12(a)), the ratio of the pressure drop of pulsating flow to the pressure drop of steady-state flow (Fig. 12(b)), and the performance coefficient with nondimensional frequency for various Reynolds number are presented in Fig. 12.

As can be seen from the Fig. 12, as the frequency increases, the Nusselt number ratio and the pressure drop ratio increase. By applying the pulsation effect, the vortex power increases, which increases the mixing and thus increases the heat
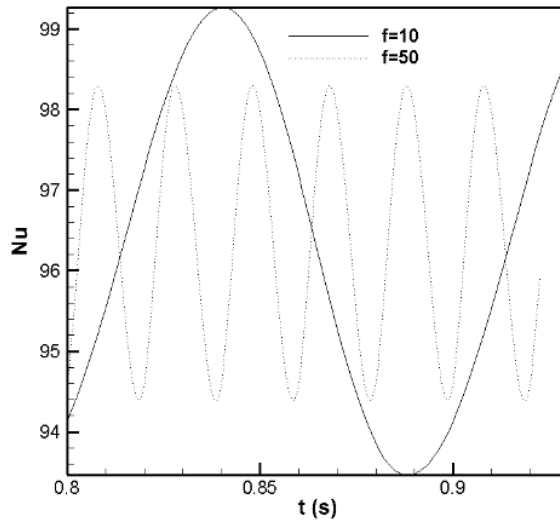
Fig. 11. Nusselt number variation with time for fluid flow inside the helical-coil tube with *d* = 9 mm and *D* = 112 mm for two frequencies of 10 Hz and 50 Hz
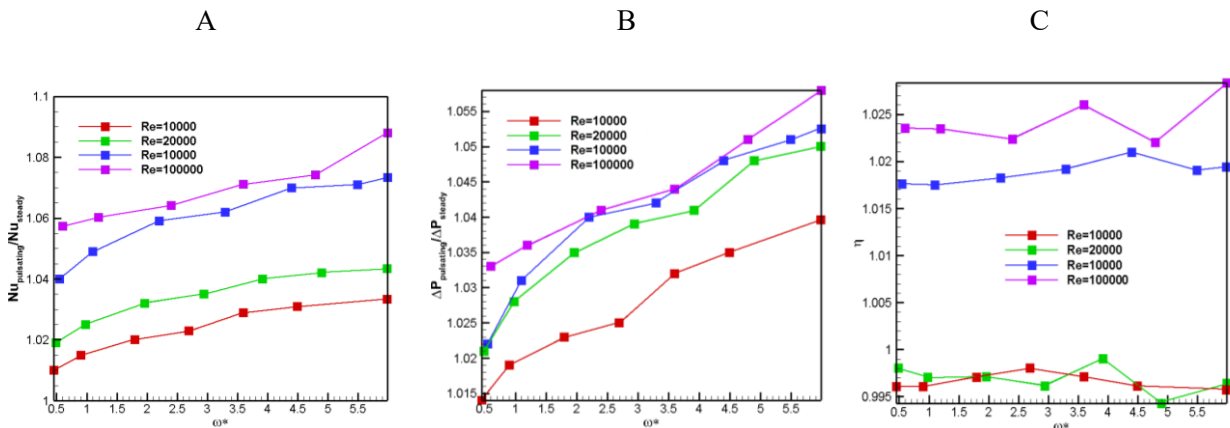

Fig. 12. A) Nusselt number of pulsation flow to that of steady-state variation, B) Pressure drop of pulsation flow to that of steady-state variation, C) Performance evaluation criteria, with nondimensional frequency for various Reynolds number of the nanofluid flow inside the helical-coil tube for *d* = 9 mm and *D* = 112 mm to the base fluid.

transfer and increases the pressure drop, too. The performance coefficient for the lower Reynolds numbers is almost constant and below 1, and for higher Reynolds numbers is increasing and higher than 1.

7. CONCLUSION

In this study, the results of the simulation of the pulsating flow inside the helical-coil tube with the constant heat flux as boundary conditions were presented and compared with the steady-state flow condition. In addition, the effect of using water/aluminum oxide nanofluid on the heat transfer and pressure drop was investigated. The flow lines for the helical-coil tube indicate that besides the main lines of the flow, which are in the direction of the main axis of the tube, a secondary flow is also formed due to the centrifugal force, which increases the heat transfer and the pressure drop. As the nanoparticles volume fraction increases, the pressure

drop and the heat transfer coefficient for the water/alumina nanofluids flow inside the helical-coil tube increases compared to the base fluid flowing inside the straight tube. The pulsating flow together with increasing the vortices due to coil tube can increase the heat transfer and pressure drop too. The increases in the heat transfer and pressure drop in pulsating flow are in competition with each other, and if each one dominates another, the performance coefficient is affected as well.

REFERENCES

[1] M. Sheikholeslami, H. Sajjadi, A. Amiri Delouei, M. Atashafrooz, Z. Li, Magnetic force and radiation influences on nanofluid transportation through a permeable media considering Al_2O_3 nanoparticles, *Journal of Thermal Analysis and Calorimetry*, 136 (6) (2019) 2477-2485.

[2] A.A. Abbasian Arani, J. Amani, M. Hemmat Esfeh, Numerical simulation of mixed convection flows in a square double lid-driven cavity partially heated using nanofluid, *Journal of Nanostructures*, 2(3) (2012) 301-311.

[3] M. Atashafrooz, M. Sheikholeslami, H. Sajjadi, A. Amiri Delouei,

Interaction effects of an inclined magnetic field and nanofluid on forced convection heat transfer and flow irreversibility in a duct with an abrupt contraction, *Journal of Magnetism and Magnetic Materials*, 478 (2019) 216-226.

[4] A.A. Abbasian Arani, E. Kakoli, N. Hajialigol, Double-diffusive natural convection of Al_2O_3-water nanofluid in an enclosure with partially active side walls using variable properties, *Journal of Mechanical Science and Technology*, 28(11) (2014) 4681-4691.

[5] H. Sajjadi, A. Amiri Delouei, M. Atashafrooz, M. Sheikholeslami, Double MRT Lattice Boltzmann simulation of 3-D MHD natural convection in a cubic cavity with sinusoidal temperature distribution utilizing nanofluid, *International Journal of Heat and Mass Transfer*, 126 (A) (2018) 489-503.

[6] M. Hemmat Esfe, A.A. Abbasian Arani, M.R. Madadi, A. Alirezaie, A study on rheological characteristics of hybrid nano-lubricants containing MWCNT-TiO_2 nanoparticles, *Journal of Molecular Liquid*, 260 (2018) 229-236.

[7] M. Atashafrooz, Effects of Ag-water nanofluid on hydrodynamics and thermal behaviors of three-dimensional separated step flow, *Alexandria Engineering Journal,* 57(4) (2018) 4277-4285.

[8] M. Hemmat Esfe, A.A. Abbasian Arani, A. Aghaie, S. Wongwises, Mixed convection flow and heat transfer in an up-driven, inclined, square enclosure subjected to DWCNT-water nanofluid containing three circular heat sources, *Current Nanoscience*, 13(3) 311-323.

[9] M. Dastmalchi, G.A. Sheikhzadeh, A.A. Abbasian Arani, Double-diffusive natural convective in a porous square enclosure filled with nanofluid, *International Journal of Thermal Sciences*, 95 (2015) 88-98.

[10] M. Hemmat Esfe, H. Rostamian, A. Shabani-samghabadi, A.A. Abbasian Arani, Application of three-level general factorial design approach for thermal conductivity of MgO/water nanofluids, *Applied Thermal Engineering*, 127 (2017) 1194-1199.

[11] A.A. Abbasian Arani, H. Aberoumand, S. Aberoumand, A.J. Moghaddam, M. Dastanian, An empirical investigation on thermal characteristics and pressure drop of Ag-oil nanofluid in concentric annular tube, *Heat and Mass Transfer*, 52 (8) (2016) 1693-1706.

[12] A.A. Abbasian Arani, S. Sadripour, S. Kermani, Nanoparticle shape effects on thermal-hydraulic performance of boehmite alumina nanofluids in a sinusoidal–wavy mini-channel with phase shift and variable wavelength, *International Journal of Mechanical Sciences*, 128-129 (2017) 550-563.

[13] H. Ramezani Kharvani, F. Ilami Doshmanziari, A. Zohir, D. Jalali-Vahid, An experimental investigation of heat transfers in a spiral-coil tube with pulsating turbulent water flow, Heat Mass Transfer, 52(9) (2015) 1179-1789.

[14] Z. Jun, Z. Danling, W. Ping, G. Hong, An Experimental Study of Heat Transfer Enhancement with a Pulsating Flow, *Heat Transfer—Asian Research*, 33 (5) (2004) 271-278.

[15] F. Doshmanziari, A. Zohir, H. Ramezani Kharvani, D. Jalali-Vahid, M. Kadivar M, Characteristics of heat transfer and flow of Al2O3/water nanofluid in a spiral-coil tube for turbulent pulsating flow, *Heat and Mass Transfer*, 52 (7) (2015) 1305-1320.

[16] A. Zohir, A. Abdel Aziz, M. Habib, Heat Transfer Characteristics and Pressure Drop of the Concentric Tube Equipped with Coiled Wires for Pulsating Turbulent flow, *Experimental Thermal and Fluid Sciences*, 65 (2015) 41-51.

[17] H. Hassanzadeh Afrouzi, A. Rabienataj Darzi, M. Delavar, A. Abouei Mehrizi, Pulsating Flow and Heat Transfer in a Helical Tube wit h Constant Heat Flux, *International Journal of Advance Industrial Engineering*, 1(2) (2013) 36-39.

[18] P. Patro, R. Gupta, A. Khuntia, Numerical Study for the prediction of heat transfer in a pulsating turbulent flow in a pipe, *Procedia Engineering*, 127 (2015) 854 – 861.

[19] P. Naphon, S. Wiriyasart, Pulsating TiO_2/water nanofluids flow and heat transfer in the spirally coiled tubes with different magnetic field directions, *International Journal of Heat and Mass Transfer*, 115 (2017) 537–543.

[20] S. Sivasankaran, K. Narrein, Numerical investigation of two-phase laminar pulsating nanofluid flow in helical microchannel filled with a porous medium, *International Communications in Heat and Mass Transfer*, 75 (2016) 86-91.

[21] M. Rahgoshay, A. Ranjbar, A. Ramiar, Laminar pulsating flow of nanofluids in a circular tube with isothermal wall, *International Communications in Heat and Mass Transfer*, 39 (2012) 463–469.

[22] Y. Ishino, M. Suzuki, N. Ohiwa, Flow and heat transfer characteristics in pulsating pipe flow (effects of pulsation on internal heat transfer in a circular pipe flow), *Heat Transfer Japanese Resarch*, 25(5) (1996) 323–341.

[23] E. Elshafei, M. Safwat Mohamed, H. Mansour, M. Sakr, NUMERICAL STUDY OF HEAT TRANSFER IN PULSATING TURBULENT AIR FLOW, *Thermal Issues in Emerging Technologies, ThETA 1*, Cairo, (2007) 63-70.

[24] M. Jarrahi, C. Castelain, Secondary flow patterns and mixing in laminar pulsating flow through a curved pipe, *Experiments in Fluids*, 50 (2010) 1539–1558.

[25] F. Selimefendigil, H.F. Öztop, Effects of phase shift on the heat transfer characteristics in pulsating mixed convection flow in a multiple vented cavity, *Applied Mathematical Modeling*, 39 (13) (2015) 3666-3677.

[26] X. Wang, N. Zhang, Numerical analysis of heat transfers in pulsating turbulent flow in a pipe, *International Journal of Heat and Mass Transfer*, 48 (19–20) (2005) 3957-3970.

[27] ANSYS CFX–solver theory guide, Release 15, in, ANSYS Inc., 2013.

[28] Ö Ağra, H. Demir, Ş.Ö Atayılmaz, F. Kantaş, A.S. Dalkılıç, Numerical investigation of heat transfer and pressure drop in enhanced tubes, *International Communications in Heat and Mass Transfer*, 38(10) (2011) 1384-1391.

[29] E. Elshafei, M.S. Mohamed, H. Mansour, M. Sakr, Experimental study of heat transfer in pulsating turbulent flow in a pipe, *International Journal of Heat and Fluid Flow*, 29(4) (2008) 1029-1038.

[30] M. Khairul, R. Saidur, M. Rahman, M. Alim, A. Hossain, Z. Abdin, Heat transfer and thermodynamic analyses of a helically coiled heat exchanger using different types of nanofluids, *International Journal of Heat and Mass Transfer*, 67 (2013) 398-403.

[31] X.Wang, N. Zhang, Numerical analysis of heat transfer in pulsating turbulent flow in a pipe, *International Journal of Heat and Mass Transfer*, 48(19-20) (2005) 3957-3970.

[32] M.A. Habib, A.M. Attya, S.A.M Said, A.L. Eid, A.Z. Aly, A.Z., Heat transfer characteristics and Nusselt number correlation of turbulent pulsating air flows, *Journal of Heat and Mass Transfer* 40 (2004) 307–318.

[33] N. Jamshidi, M. Farhadi, D.D. Ganji, K. Sedighi, Experimental analysis of heat transfer enhancement in shell and helical tube heat exchangers, *Applied Thermal Engineering*, 51(1-2) (2013) 644-652.

[34] M. Fakoor Pakdaman, M.A. Akhavan-Behabadi, P. Razi, An experimental investigation on thermo-physical properties and overall performance of MWCNT/heat transfer oil nanofluid flow inside vertical helically coiled tubes, *Experimental Thermal and Fluid Sciences*, 40 (2012) 103-111.

[35] M. Corcione, Empirical correlating equations for predicting the effective thermal conductivity and dynamic viscosity of nanofluids, *Energy Conversion and Management*, 52(1) (2011) 789-793.

[36] C. Ho, W. Liu, Y. Chang, C. Lin, Natural convection heat transfer of alumina-water nanofluid in vertical square enclosures: an experimental study, *International Journal of Thermal Sciences*, 49(8) (2010) 1345-1353.

[37] A. Bejan, Convection heat transfer, 2nd Edition, *Wiley*, New York, 1995.